Pericyte Bridges in Homeostasis and Hyperglycemia

Bruce A. Corliss,[1] H. Clifton Ray,[1] Richard W. Doty,[1] Corbin Mathews,[1] Natasha Sheybani,[1] Kathleen Fitzgerald,[1] Remi Prince,[1] Molly R. Kelly-Goss,[1] Walter L. Murfee,[2] John Chappell,[3] Gary K. Owens,[4] Paul A. Yates,[1,5] and Shayn M. Peirce[1,5]

Diabetes 2020;69:1503–1517 | https://doi.org/10.2337/db19-0471

Diabetic retinopathy is a potentially blinding eye disease that threatens the vision of one-ninth of patients with diabetes. Progression of the disease has long been attributed to an initial dropout of pericytes that enwrap the retinal microvasculature. Revealed through retinal vascular digests, a subsequent increase in basement membrane bridges was also observed. Using cell-specific markers, we demonstrate that pericytes rather than endothelial cells colocalize with these bridges. We show that the density of bridges transiently increases with elevation of Ang-2, PDGF-BB, and blood glucose; is rapidly reversed on a timescale of days; and is often associated with a pericyte cell body located off vessel. Cell-specific knockout of KLF4 in pericytes fully replicates this phenotype. In vivo imaging of limbal vessels demonstrates pericyte migration off vessel, with rapid pericyte filopodial-like process formation between adjacent vessels. Accounting for off-vessel and on-vessel pericytes, we observed no pericyte loss relative to nondiabetic control retina. These findings reveal the possibility that pericyte perturbations in location and process formation may play a role in the development of pathological vascular remodeling in diabetic retinopathy.

Chronic hyperglycemia associated with diabetes has long been known to cause widespread tissue damage and dysfunction across a number of end organs including kidney (1), skeletal muscle (2), liver (1), brain (1), heart (3), and retina (1). In the retina, such pathology is mediated in part through dysfunction in the many cell types that form the neurovascular unit (4). One of the earliest insults observed in these tissues is the loss of pericytes, cells that enwrap the microvasculature and support underlying endothelial cells, with this loss compromising vascular integrity (5) and leading to the eventual destruction of the microvasculature (6). Yet the reasons that pericytes are particularly susceptible to hyperglycemic injury, as compared with other cell types of the neurovascular unit, remain unclear (1).

Understanding the mechanisms that underlie this early pericyte dysfunction remains of paramount importance given that one-ninth of the 285 million patients with diabetes worldwide have vision-threatening diabetic retinopathy (7). Pericytes are considered an effector cell for microvascular remodeling and enwrap capillaries, maintaining close physical contact via cell soma and extended cellular processes within the vascular basement membrane (6). Interestingly, studies examining early vascular dysfunction have observed pericyte-like cells bridging across two or more adjacent capillaries, with dramatic increases in the number of bridges in hyperglycemic compared with homeostatic conditions (8,9). However, the cellular origin and function of such bridging cells and their implication in diabetic vascular dysfunction have not yet been established.

One hypothesis is that these pericyte-like bridges form as a result of pericyte detachment (9–12), where it is assumed that a fully attached pericyte migrates (or begins to migrate) away from the capillary on which it resides and extends cell processes or its entire cell soma to form a bridge from one capillary to another. Alternatively, other cell types may potentially give rise to these bridging cells or

[1]Department of Biomedical Engineering, University of Virginia, Charlottesville, VA
[2]Department of Biomedical Engineering, University of Florida, Gainesville, FL
[3]Fralin Biomedical Research Institute, Virginia Polytechnic Institute and State University, Blacksburg, VA
[4]Robert M. Berne Cardiovascular Research Center, University of Virginia, Charlottesville, VA
[5]Department of Ophthalmometry, University of Virginia School of Medicine, Charlottesville, VA

Corresponding author: Shayn M. Peirce, shayn@virginia.edu

Received 29 May 2019 and accepted 17 April 2020

This article contains supplementary material online at https://doi.org/10.2337/figshare.12145425.

contribute to these basement membrane bridges (8). Limited studies to date indicate that these bridging cells can colocalize with basement membrane structures that span across, or bridge, adjacent capillaries (8,13). Accordingly, these stand-alone (i.e., cell-free) basement membrane structures have, at times, been classified as collapsed acellular capillaries (14), intervascular bridges (8), basal lamina and collagen-IV (Col-IV) sleeves (15), and string vessels (14). They also appear more frequently in pathological settings than in homeostasis, and some have presumed these basement membrane bridges to be residual structures left by collapsed and regressed capillaries (review in 14).

Taken together, these observations raise numerous questions about the origin, significance, longevity, and reversibility of these cellular and acellular cross-capillary bridges. Bridge formation may provide a key insight into the early compromise of these cells and open up potential new therapeutic approaches for diabetic vascular disease. If this enriched bridging cell behavior could be reversed, with return of the pericyte cell body to the perivascular space, it would potentially offer a new means to protect existing diabetic vasculature, preventing further pericyte and vascular loss. The goal of the present studies was to examine whether pericyte detachment from the microvasculature and formation of cellular bridges are potentially key early events in diabetes that may set the stage for subsequent vascular compromise. We establish the phenotypic identity of these cell bridges using immunolabeling for Myh11, a pericyte-specific marker, and then confirmed these results using a lineage-tracing genetic reporter driven by the Myh11 promoter (16). Next, we tested whether pericyte bridges could be reversibly enriched through acute elevation of blood glucose or delivery of exogenous chemokines known to be elevated in the diabetic microenvironment (17,18). Finally, we examined a pericyte-specific knockout of KLF4, known to regulate cell migration (19), to determine its potential impact on bridge formation and its ability to replicate the phenotype of diabetic models. These initial studies allowed us to confirm a likely pericyte origin to these cellular bridges; demonstrate that the total number of pericytes remains static in early diabetic models, varying only by the distribution of on-vessel versus off-vessel pericytes; and, most importantly, demonstrate that this off-vessel bridging cell behavior can be acutely and rapidly reversed, providing a potential new mechanism for pericyte compromise and therapeutic approach for ameliorating diabetic vascular dysfunction.

RESEARCH DESIGN AND METHODS

Mouse Strains and Protocol

All procedures were approved by the Institutional Animal Care and Use Committee at the University of Virginia and completed in accordance with our approved protocol under these guidelines and regulations. With the lineage tracing and live imaging, *Myh11*-CreER^{T2} ROSA floxed STOP tdTomato mice were used, bred from *Myh11*-CreEr^{T2} mice (cat. no. 019079; The Jackson Laboratory, Bar Harbor, ME) and ROSA floxed STOP tdTomato mice (007914; The Jackson Laboratory), all on C57BL/6J background. Selective knockout of KLF4 in Myh11-expressing cells was investigated with *Myh11*-CreER^{T2} ROSA floxed STOP eYFP *Klf4*$^{fl/lf}$ with *Myh11*-CreER^{T2} ROSA floxed STOP eYFP *Klf4*$^{WT/WT}$ used as control, graciously provided by the Gary Owens laboratory (University of Virginia); mice were treated with tamoxifen as previously described (20) (Supplementary Material). All other mice used were C57BL/6J (000664; The Jackson Laboratory).

Streptozotocin (STZ)-induced diabetes was initiated as previously described (21) (Supplementary Material). Mice were injected intravitreally with Ang2 or PDGF-BB (Supplementary Material) and were examined at day 4 and additionally at day 28: long after exogenous protein had dissipated based on the short half-lives of Ang2 (22) and PDGF-BB (23). As a chronic model of type 1 diabetes, C57BL/6-Ins2Akita/J (10) mice were acquired (cat. no. 003548; The Jackson Laboratory) and harvested at 8 months of age (9). Mice were sacrificed and immunostained using previously developed techniques (24,25) (See Supplementary Material and Supplementary Tables 1 and 2 for antibodies used).

Quantifying Microvascular Structure and Pericyte Phenotype

Cell counts of pericyte association state with the vasculature (26) were quantified using Fiji's Cell Counter plugin (27) in a blinded fashion. Vessel structure was analyzed with software written in MATLAB using previously developed software (28). The deep retina vasculature was characterized because there was a higher frequency of basement membrane bridges found in homeostasis and diabetes, and the homogenous flat structure of this layer enabled consistent visualization with imaging.

Data Acquisition, Statistics, and Sampling

Two-tailed tests were used with significance level set to $\alpha = 0.05$. See figures for statistical tests and sampling.

Data and Resource Availability

The data sets generated and analyzed during the current study are available from the corresponding author upon reasonable request. Code and instructions used to quantify images are written in MATLAB and available from https://github.com/uva-peirce-cottler-lab/public_avaper. The mouse strains analyzed during the current study are either commercially available or available through the laboratories that generated them.

RESULTS

Pericyte Marker NG2 Colocalizes With Basement Membrane Bridges in Homeostasis

Previous research showed that basement membrane bridges were found in healthy homeostatic conditions in the retina (8), suggesting some form of ongoing remodeling of the basement membrane. We hypothesized that in

the homeostatic retina, endothelial cells were not colocalized with these structures, while pericytes were. Immunostaining of retinal digests, an assay used to isolate the vasculature via enzymatic digestion where only endothelial cells, pericytes, and basement membrane bridges remain (9), revealed that these thin basement membrane structures are Col-IV$^+$ but negative for pan-endothelial marker CD31 (29) and retina-specific endothelial marker CD105 (30) (Fig. 1*A–D*), confirming previous findings (29). In whole mount immunostained retinas, these Col-IV$^+$ bridges also colabeled with other markers of the basement membrane, including fibronectin, laminin, and IB4 lectin (Fig. 1*E–G*). These basement membrane bridges, and the associated cell soma often found connected to them, appeared to morphologically match the thin fibrous structures that have previously been referred to as collapsed acellular capillaries in nonspecific cell staining of retinal digests (14) (Fig. 1*H* and *I*).

When the retina of an adult human without diabetes was examined, basement membrane bridges connecting neighboring capillaries were observed, including a collapsed acellular capillary marked by a thin basement membrane bridge (14) (Fig. 2*A–C*) and a thicker acellular capillary with a diameter at least 20% of surrounding capillaries (29,31) (Fig. 2*D–F*). When the diameter of basement membrane segments was compared between those that colabel with CD31 (capillary, 9.55 ± 1.39 μm) and those that do not (basement membrane bridge, 4.32 ± 2.03 μm), there was a marked degree of separation between groups, with a 54.8% reduction in diameter from capillary segments (P = 1.63E-10). When basement bridges were separated as those that contain a Col-IV lumen colabeled with CD31 (capillary, 9.55 ± 1.39 μm), those that contain a lumen with no CD31 expression (basement membrane bridge with Col-IV lumen, 6.85 ± 1.21 μm), and those lacking both a lumen and CD31 expression (basement membrane bridge without lumen, 3.21 ± 1.08 μm), there was again a distinct separation (53.1% reduction from basement bridges with lumens compared with those without, P = 1.29E-4).

We examined healthy murine tissue and characterized these structures in the deep retinal plexus. Representative images of immunostaining of homeostatic retina (Fig. 3*A*) revealed capillaries and off-vessel bridges labeled with Col-IV$^+$ basement membrane, as well as no signs of vessel formation or regression, as expected in homeostasis. Similarly to what was observed in human retina, when the diameter of basement membrane segments of the microvascular network was grouped based on marker expression, Col-IV segments with CD31/CD105 endothelial expression measured 5.64 ± 0.08 μm in diameter, while nonendothelial segments had a 60.5% reduced diameter of 2.23 ± 0.08 μm (P = 2.99E-12) (Fig. 3*B*), suggesting that these features of the vasculature network may represent distinct structures. In contrast with human retinal vasculature, we observed no basement membrane bridges in mouse retina that contained any sign of a Col-IV lumen. In further support that endothelial cells do not coincide with basement bridge structures, when the marker expression of Col-IV$^+$ basement membrane bridge segments was examined (diameter <3.5 μm to exclude capillaries, determined by Fig. 3*B*), none of the segments colabeled with endothelial cell markers, while 20.5 ± 1.4% of them colabeled with NG2 (denoting the presence of an active pericyte cell process) and 79.5 ± 1.4% colabeled with neither (P = 3.70E-27) (Fig. 3*C*). While a unique pericyte marker does not currently exist, NG2 has previously been used to label retinal pericytes (32), and here we combined NG2 with Col-IV basement membrane for analysis of pericyte morphologies.

A range of NG2$^+$ cell morphologies was found, which we classified as either an attached pericyte with cell soma and all cell processes associated with a vessel (Fig. 3*D* and *E*) or a pericyte bridge with a cell soma or process extending partially off vessel (Fig. 3*F–H*). Additionally, we divided attached pericytes into a subgroup with those that are connected by an off-vessel basement membrane bridge (basement-bridged pericyte) that lack colabeling with pericyte and endothelial cell markers, giving an impression of a cell-free basement membrane track (Fig. 3*E*).

Pericyte Bridges Express the Smooth Muscle Cell– and Pericyte-Specific Marker Myh11

Previously, the myosin heavy chain 11 (Myh11) promotor has been used in an inducible lineage–tracing reporter mouse model to track the lineage of smooth muscle cells (33). Myh11 lineage cells also colabeled with the majority of NG2- or PDGFRβ-expressing pericytes (16) and have been used to study them. We hypothesized that pericyte bridges would be marked in this mouse model and that the exclusivity of Myh11 expression could be leveraged to visualize pericyte morphology with higher confidence of cell identity than with NG2 or PDGFRβ as markers. Post–tamoxifen induction in the *Myh11*-CreER^{T2} ROSA floxed STOP tdTomato (Myh11-RFP) mouse model in the deep retinal plexus, RFP$^+$ Myh11 lineage [Myh11-Lin(+)] cells colabeled with NG2$^+$ cells that bridged between blood vessels marked with CD31 (Fig. 4*A* and *B*), CD34, and CD105 (Supplementary Fig. 1*A* and *B*). Since RFP expression denoted Myh11 expression induced during the tamoxifen treatment period ending 4 weeks prior to sacrifice, these Myh11-Lin(+) cells could have lost Myh11 expression during the chase period. However, we found that these bridging cells are also labeled when immunostained for the Myh11 protein (Fig. 4*C*). The fact that Myh11 expression was found in these bridging cells in tandem with NG2 expression and colocalized with a Col-IV$^+$ basement membrane argued that pericyte bridges maintained their pericyte identity and Myh11 can serve as a marker that includes this pericyte subpopulation. Leveraging the ability of this mouse model to label pericyte bridges endogenously, we observed pericyte bridges in other tissues (Fig. 4*D–K*), suggesting that this morphology represents a fundamental pericyte phenotype found across vascularized tissues.

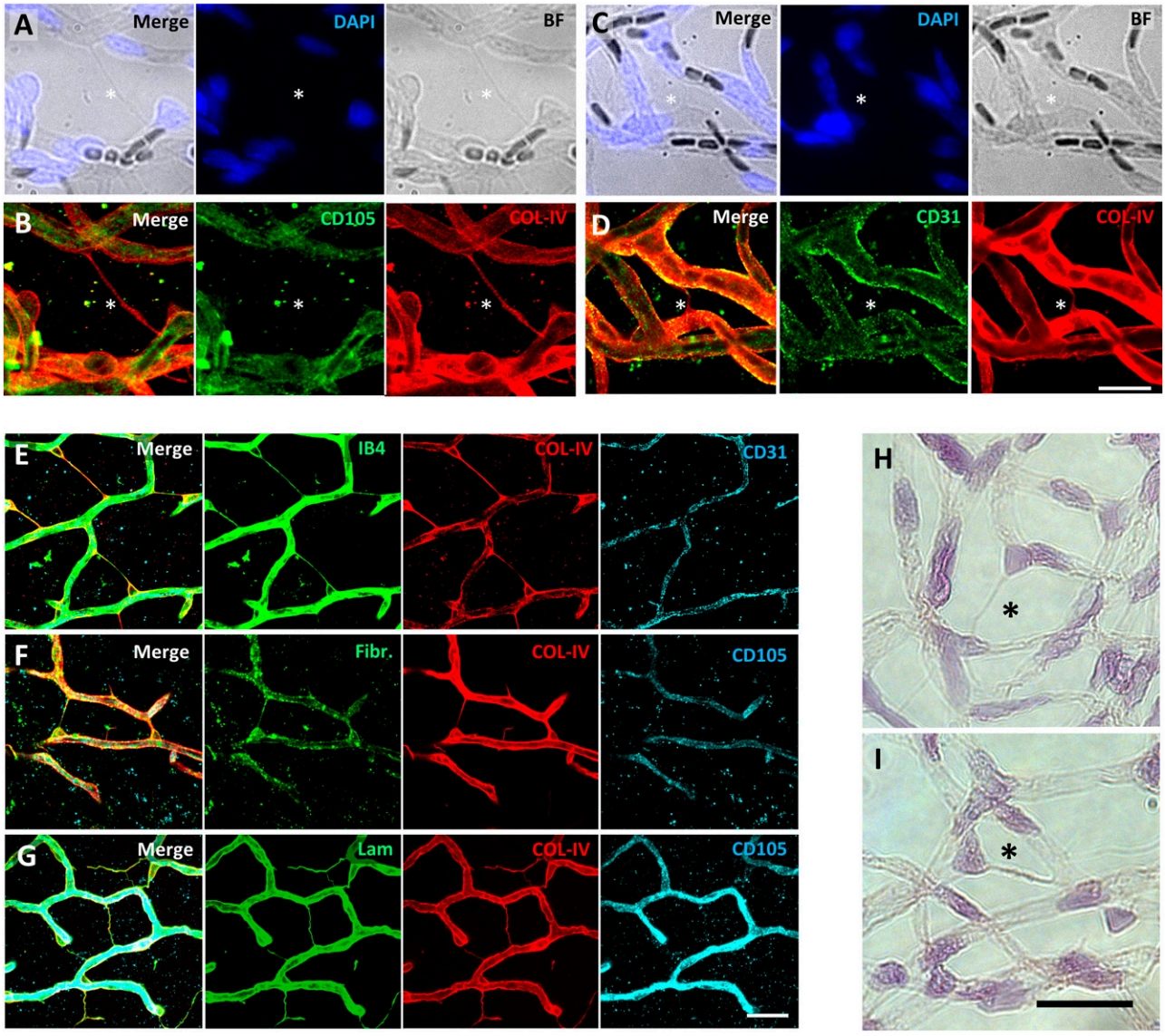

Figure 1—Acellular capillaries in murine retina colabel with basement membrane markers but lack endothelial markers. *A* and *B*: Brightfield (BF) image of acellular capillary (*) between two fully formed capillaries (*A*) with field of view imaged fluorescently with anti-CD105 (green) and anti–Col-IV (red) (*B*). *C* and *D*: Brightfield of acellular capillary (*) (*C*) with same location fluorescently imaged with anti-CD31 (green) and anti–Col-IV (red) (scale bar, 15 μm) (*D*). *E*: Fluorescent confocal image of whole mount retina in deep plexus stained with isolectin IB4 (green), anti–Col-IV (red), and anti-CD31 (cyan). *F*: Retinal deep plexus labeled with anti-fibronectin (Fibr.) (green), anti–Col-IV (red), and anti-CD105 (cyan). *G*: Retinal deep plexus labeled with anti-laminin (Lam) (green), anti–Col-IV (red), and anti-CD105 (cyan) (scale bar, 25 μm). *H* and *I*: Transmission light image of retinal digest stained with hematoxylin-eosin, with structures previously referred to as acellular capillaries (*) (scale bar, 15 μm).

Short-term and Long-term Hyperglycemia Elevates, While Insulin Treatment Reduces, Pericyte Bridge Density in STZ-Induced Diabetes

Published data from retinal digests suggested that basement and pericyte bridges were enriched over the course of months in diabetic conditions (34), yet it remains unknown whether they form over the short-term prior to other observed microvascular remodeling events in diabetes. We examined whether acute short-term hyperglycemia can modulate bridge density in a reversible fashion by imaging the deep plexus retinal vasculature 1 week and 2 weeks post–STZ treatment, post–STZ treatment with sustained insulin treatment via subcutaneous osmotic pump, and post–vehicle control (Fig. 5*A*). Mice with STZ-induced diabetes had a 20.9% increase in enriched pericyte bridge density (fraction of pericytes with an off-vessel bridging phenotype) compared with vehicle at day 7 (Fig. 5*B*) mirrored by a 4.3% reduction in attached pericyte density ($P = 4.27E\text{-}3$) (Fig. 5*C*). At day 14, pericyte bridges in diabetic mice were enriched 50.5% and attached pericytes decreased 13.8% ($P = 4.65E\text{-}8$). Insulin treatment conferred partial rescue, leading to a 49.3%

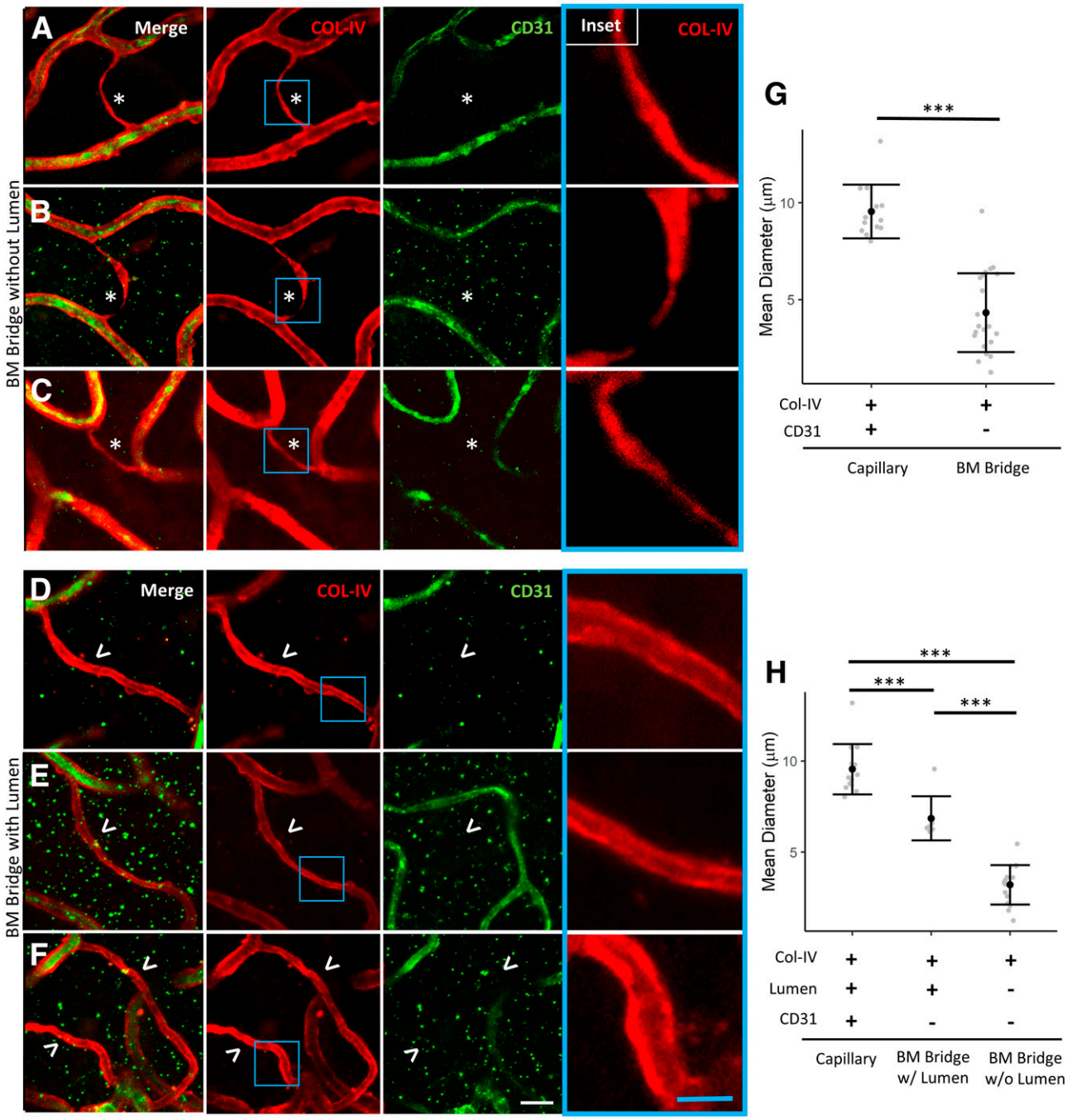

Figure 2—Human retinal vasculature contains two classes of basement membrane (BM) bridges distinguished based on thickness and the presence of a basement membrane lumen. *A–C*: Representative images of thin basement membrane bridges (*) that connect capillaries (CD31 [green]) and lack any sign of Col-IV lumen (red). *D–F*: Representative images of basement membrane bridges (arrow) that connect capillaries (CD31 [green]) and contain a Col-IV lumen (red) (white scale bar, 25 μm; blue box outlines inset with blue scale bar, 10 μm). *G*: Comparison of diameter of basement membrane segments that colabel with CD31 (capillary, $n = 13$) and those that do not (basement membrane bridge, $n = 23$) (Welch *t* test; $N = 1$ retina). *H*: Comparison of diameter of basement membrane segments with a Col-IV lumen colabeled with CD31 (capillary, $n = 13$), a Col-IV lumen with no CD31 expression (basement membrane bridge with lumen, $n = 7$), and a segment lacking both a Col-IV lumen and CD31 expression (basement membrane bridge without lumen, $n = 13$) (one-way ANOVA with Tukey-Kramer multiple comparison; $N = 1$ retina). ***$P < 0.001$. w, with; w/o, without.

reduction in pericyte bridge density compared with untreated diabetic mice, along with 8.3% increase in attached pericytes ($P = 3.90E-5$). We observed a similar trend toward enriched basement-bridged pericytes with STZ treatment at day 7 (Fig. 5*D*) and a 34.9% increase in density at day 14 ($P = 7.21E-5$), along with a trend toward 28.2% reduction with insulin treatment compared with in the untreated diabetic condition ($P = 6.68E-2$). However,

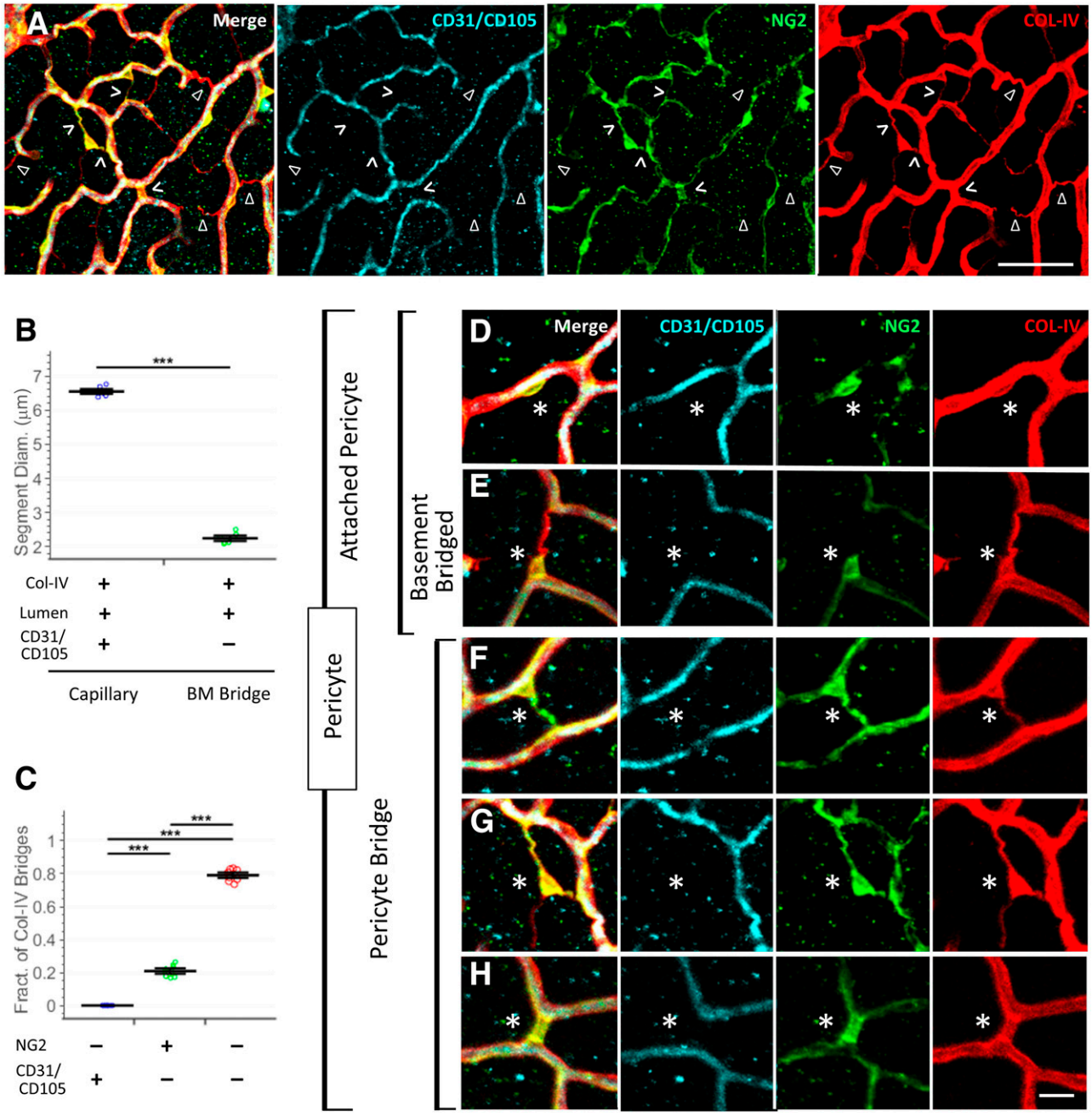

Figure 3—Basement membrane bridges, a subset of which colabel with the pericyte marker NG2, represent distinct morphological structures compared with lumenized vessels. *A*: Various off-vessel Col-IV tracks (red, closed arrow) are observed bridging CD31/CD105 blood vessels (cyan) in deep plexus of the retina, a subset of which colabel with NG2 (green, open arrow) (scale bar, 50 μm). *B*: Comparison of diameter (Diam.) of Col-IV segments that colabel with and without the endothelial markers CD31 and CD105 (Welch *t* test; $N = 6$ mice, $n = 3$ images/mice). *C*: Fraction (Fract.) of colabeled basement membrane (BM) bridges (Col-IV structures <3.5 μm diameter) that colabel with pericyte marker NG2, endothelial markers CD31/CD105, and neither (one-way Kruskal Wallis with Bonferroni correction, $N = 6$ mice). Classification with abbreviations of various pericyte phenotypes (*) in relation to the vascular network, including a fully attached pericyte, some of which are connected to empty basement membrane bridges (*D* and *E*), and various types of pericyte bridges (*F–H*) (scale bar, 15 μm). ***$P < 0.001$.

there was no change between diabetic and vehicle mice in the total $NG2^+$ pericyte population for days 7 ($P = 0.653$) (Fig. 5*E*) and 14 ($P = 0.510$). Basement membrane bridges marked with Col-IV, along with the subset of those that were colabeled with NG2, displayed the same trends as pericyte bridges with diabetes and insulin treatment (Fig. 5*F* and *G*). There was no evidence of angiogenesis or regression, with no changes to vessel length density (day 7 $P = 0.848$, day 14 $P = 0.599$) (Fig. 5*H*), branch points per vessel length (day 7 $P = 0.987$, day 14 $P = 0.712$) (Fig. 5*I*), and segment tortuosity (day 7 $P = 0.131$, day 14 $P = 0.244$) (Fig. 5*J*). In support of perivascular

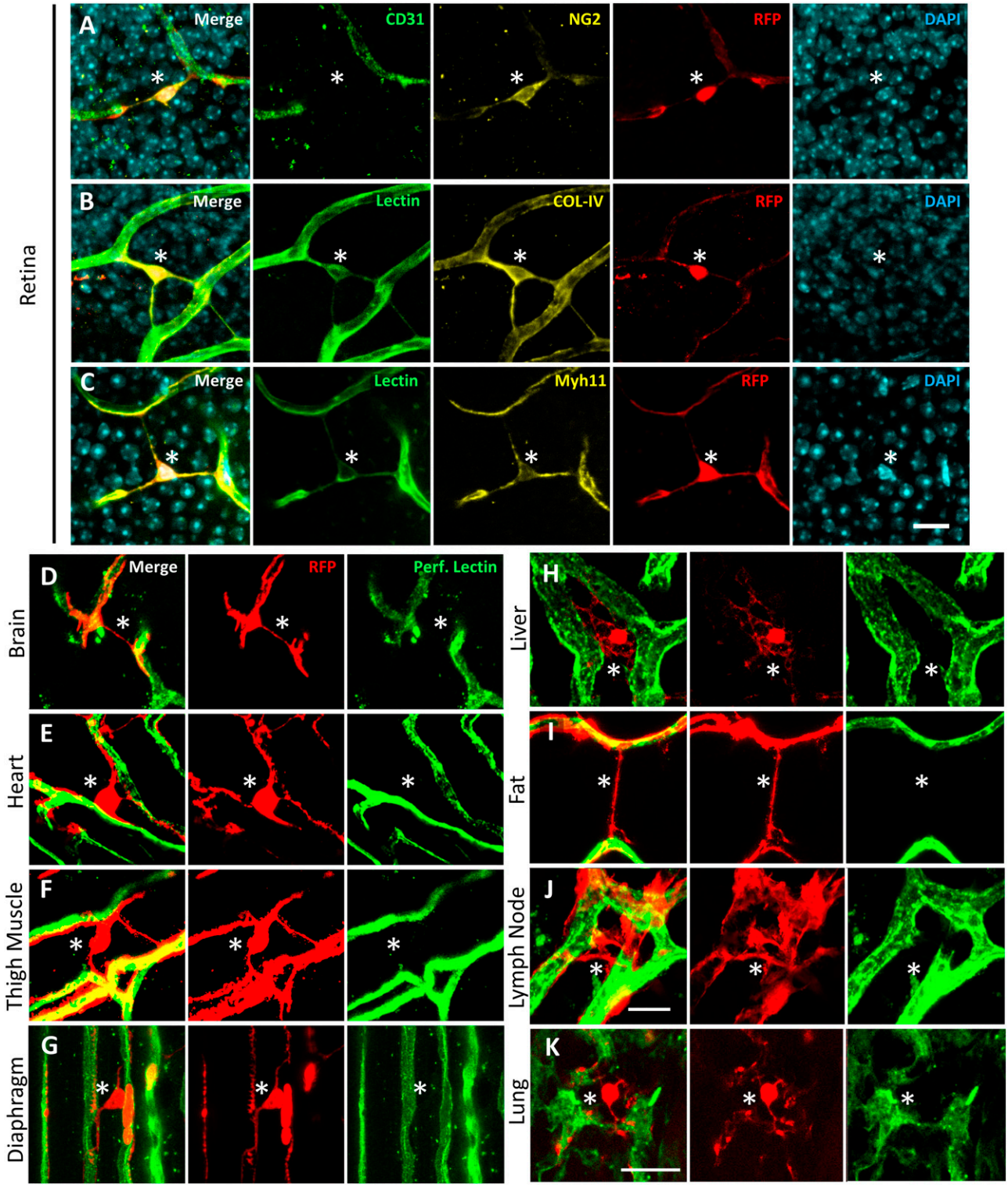

Figure 4— Pericyte bridges express Myh11, are of Myh11 lineage, and are found across various tissues in quiescence. *A*: Pericyte bridge (*) of Myh11 lineage labeled with anti-CD31 (green), anti-NG2 (yellow), anti-RFP (red), and DAPI (cyan). *B*: Pericyte bridge labeled with IB4 lectin (green), anti–Col-IV (yellow), anti-RFP (red), and DAPI (cyan). *C*: Pericyte bridge labeled with IB4 lectin (green), anti-Myh11 (yellow), anti-RFP (red), and DAPI (cyan) (scale bar, 15 μm). Myh11-lineaged RFP^+ cells (red) imaged with perfused IB4 lectin (green) in brain (*D*), heart (*E*), thigh muscle (*F*), diaphragm (*G*), liver (*H*), inguinal fat (*I*), lymph node (*J*), and lung (*K*) (scale bar, 15 μm).

remodeling, the density of pericyte bridges, basement-bridged pericytes, and off-vessel bridges all correlated with mouse blood glucose levels at the time of sacrifice across groups and time points (Supplementary Fig. 2*D–G*). Blood glucose and mouse weight confirmed hyperglycemia for each study group (Supplementary Fig. 2*A–C*); representative images of retinas harvested from hyperglycemic and control mice at days 7 (Supplementary Fig. 2*H* and *I*) and 14 (Fig. 5*L–O*) are provided. Similar patterns were observed with hyperglycemia over the longer term of 3.5 months with STZ-induced diabetes (Supplementary Fig. 3*A–Q* and Supplementary Fig. 4*A–C*) and with genetic knockout of insulin in the Akita mouse strain (10) at 8 months of age (Supplementary Fig. 5*A–L*). Across both models and time points, we observed no basement membrane bridges that contained any sign of a Col-IV lumen.

Injection of Recombinant PDGF-BB and Ang2 Transiently Elevates Pericyte Bridge Density

Platelet-derived growth factor BB (PDGF-BB), a pericyte chemokine elevated in diabetes (35), binds to PDGFRβ expressed by pericytes but not endothelial cells (36). We hypothesized that addition of exogenous PDGF-BB would result in an enriched density of pericyte bridges with no change to total pericyte density. Four days post–PDGF-BB injection (Fig. 6*A*), pericyte bridge density was enriched 47.1% (Fig. 6*B*) and attached pericytes reduced 19.2% relative to vehicle control ($P = 2.39E-5$) (Fig. 6*C*). At day 28, pericyte bridge density recovered to basal levels compared with control with a trending increase of 11.0%, while attached pericytes were qualitatively reduced 2.2% ($P = 0.0866$). In contrast, following Ang2 stimulus, basement-bridged pericyte density was reduced 57.5% at day 4 compared with control ($P = 1.65E-3$) (Fig. 6*D*) and restored by day 28 ($P = 0.770$). Total NG2-labeled cell density remained constant at both days 4 ($P = 0.583$) (Fig. 5*E*) and 28 ($P = 0.342$). Col-IV bridges and the subset colabeled with NG2 followed trends similar to pericyte bridge density across study groups (Fig. 6*F* and *G*). No angiogenesis was observed per vessel length density ($P = 0.459$) (Fig. 6*H*), a modest 11.7% increase was observed in branch points per vessel length ($P = 0.0147$) (Fig. 6*I*), and no change was observed in segment tortuosity ($P = 0.202$) (Fig. 6*J*). Representative images at days 4 (Fig. 6*L* and *M*) and 28 (Supplementary Fig. 7*A* and *B*) are provided. Similar patterns were observed following injection of Ang2 (Supplementary Fig. 6*A–L*, Supplementary Fig. 7*C* and *D*, and Supplementary Material). Across both models and all time points, none of the basement membrane bridges contained a Col-IV lumen.

Knockout of KLF4 Results in Elevated Pericyte Bridge Density

In vascular smooth muscle cells, KLF4 can negatively regulate cell migration (19,37), and in Myh11-lineaged cells it has been shown to alter smooth muscle cell phenotype (20). To elucidate a possible molecular mechanism that modulates pericyte bridge formation, we characterized mice with Myh11 lineage–specific inducible KLF4-KO (Myh11-$Cre^{Ert}EYFP^{+/+}KLF4^{fl/fl}$) relative to wild-type (WT) (Myh11-$Cre^{Ert}EYFP^{+/+}KLF4^{WT/WT}$) littermate control mice (Fig. 7*A*). YFP^+ pericyte bridges were enriched by 48.2% in the deep plexus of homeostatic retina in KLF4-KO mice compared with WT (Fig. 7*B*), while YFP^+ attached pericytes were reduced by 8.7% ($P = 1.22E-5$) (Fig. 7*C*). YFP^+ basement-bridged pericytes were enriched 41.5% within KLF4-knockout retinas ($P = 1.61E-3$) (Fig. 7*D*). YFP^+ cell density was not altered in the knockout mice ($P = 0.699$) (Fig. 7*E*). The density of laminin bridges and the subset colabeled with YFP followed trends similar to that of pericyte bridge density across study groups (Fig. 7*F* and *G*). There was no evidence of angiogenesis as measured by vessel length density ($P = 0.451$) (Fig. 7*H*) and no change to branch points per vessel length ($P = 0.395$) (Fig. 7*I*) or enriched vessel segment tortuosity in the knockout ($P = 7.27E-3$) (Fig. 7*J*). Representative images are shown at 14 weeks of age (Fig. 7*K* and *L*), 6 weeks after tamoxifen treatment was completed. Basement membrane bridges did not contain a Col-IV lumen.

Pericytes Are Capable of Migration and Process Extension, Revealed Through In Vivo Time Lapse

While population-level analysis has previously suggested that pericyte bridges could be formed by active cell movement, there is a lack of evidence directly demonstrating that pericytes can migrate or extend off-vessel processes. As a requirement for pericyte remodeling, we investigate whether pericytes are capable of dynamic process extension and migration off vessel and explored this through in vivo time lapse imaging of corneal limbal vessels, a vascular bed bordering the sclera and cornea noted for its utility in live imaging (38). For provision of an angiogenic response mimicking that in diabetic retinopathy, silver nitrate burns were applied to the Myh11-RFP mouse cornea (38), followed by pericyte tracking with the vascular perfusion of IB4 lectin to label vessels. At day 2 post–cornea burn, prior to when the majority of angiogenesis initiates in the model (39), we observed multiple RFP^+ cell somas migrating off the perfused vasculature (Fig. 8*A–C*) or RFP^+ cell processes extending off vessel (Fig. 8*D*), confirming our hypothesis that pericytes are capable of undergoing migration and process extension dynamically in adult tissue.

DISCUSSION

For the last half century (40), pericyte loss has been theorized to be a significant driver of microvascular damage (17) and eventual loss of vision (41). The reduction in pericyte density, established over many decades, is presumed to be from the toxic effects of hyperglycemia precipitating cell death (42) or from pericyte migration, but with the latter presented as an alternative hypothesis with

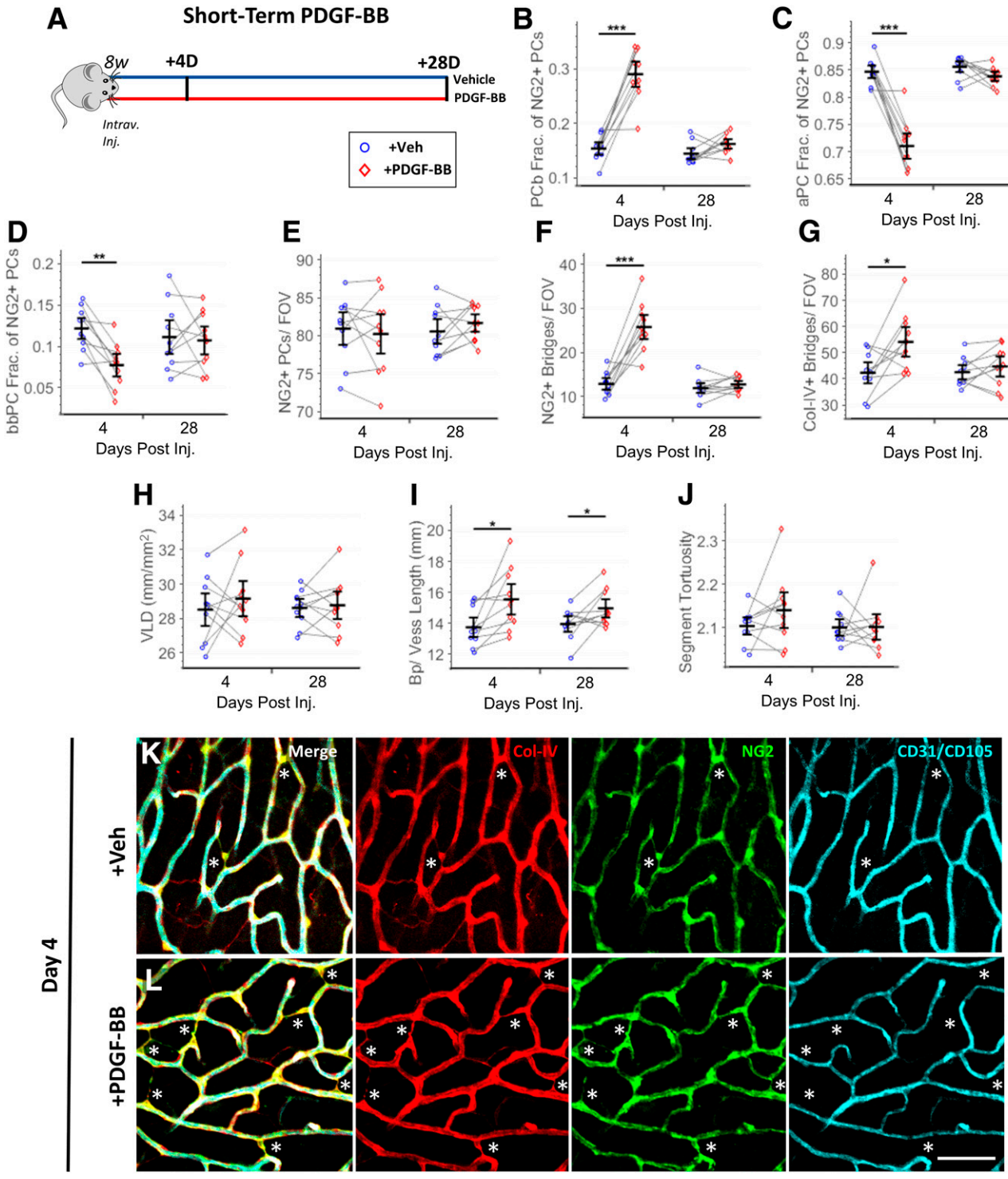

Figure 5—Short-term STZ-induced hyperglycemia enriched pericyte bridge density and was normalized with short-term insulin treatment over a static vessel network structure. *A*: Experiment design. In the deep retinal plexus, quantification of pericyte morphology, including fraction of NG2$^+$ pericytes with pericyte bridge phenotype (*B*), fraction of NG2$^+$ pericytes with attached pericyte phenotype (*C*), fraction of NG2$^+$ pericytes with basement-bridged phenotype (*D*), total NG2$^+$ pericytes per field of view (*E*), NG2$^+$ bridges per field of view (*F*), and all Col-IV$^+$ bridges per field of view (*G*) (day 7, unpaired *t* test; day 14, one-way ANOVA with Tukey multiple comparisons; $N = 9$ mice, $n = 5$ images/mice, field of view 530 μm). Vessel network morphology quantified with vessel length density (VLD) (mm/mm^2) (*H*), branch points per vessel length (Bp/Vess length) (*I*), and vessel segment tortuosity (*J*). *K–M*: Representative images of retinal deep plexus at day 14 from each treatment group, with anti–Col-IV (red) and anti-NG2 (green), along with anti-CD31 and anti-CD105 (cyan), with annotated pericyte bridges (*) (scale bar, 50 μm). *$P < 0.05$; **$P < 0.01$; ***$P < 0.001$. aPC, attached pericyte; bbPC, basement-bridged pericyte; FOV, field of view; Frac., fraction; Intrav. Inj., intravitreal injection; PCb, pericyte bridge; PCs, pericytes; Post Inj., post-injection; Veh, vehicle.

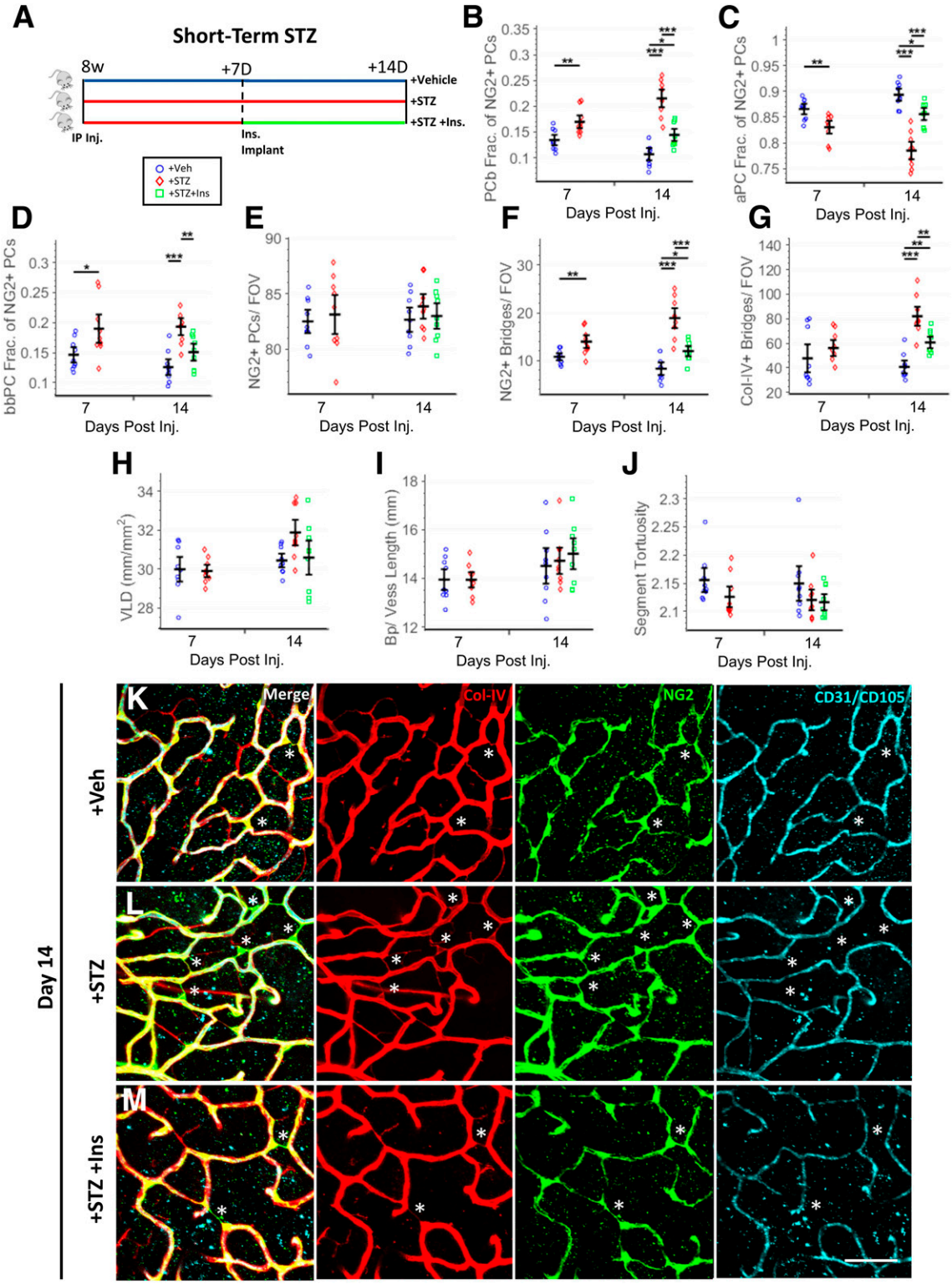

Figure 6—Intravitreal injection of PDGF-BB transiently enriched pericyte bridge density over a morphologically static vessel network. *A*: Experiment design with Vehicle (Veh), STZ, and insulin (Ins) treatments. In the deep retinal plexus, quantification of pericyte morphology, including fraction of $NG2^+$ pericytes with pericyte bridge phenotype (*B*), fraction of $NG2^+$ pericytes with attached pericyte phenotype (*C*), fraction of $NG2^+$ pericytes with basement-bridged phenotype (*D*), total $NG2^+$ pericytes per field of view (*E*), $NG2^+$ bridges per field of view (*F*), and all Col-IV^+ bridges per field of view (*G*) (paired *t* test at each time point; $N = 10$ mice, $n = 4$ images/eye, 530 μm field of view). Vessel network morphology quantified with vessel length density (mm/mm^2) (*H*), branch points per vessel length (*I*), and vessel segment tortuosity (*J*). *K* and *L*: Representative images of retinal deep plexus at day 4 from each treatment group stained with anti-Col-IV (red) and anti-NG2 (green), along with anti-CD31 and anti-CD105 (cyan), with annotated pericyte bridges (*) (scale bar, 50 μm). $^*P < 0.05$; $^{**}P < 0.01$; $^{***}P < 0.001$. aPC, attached pericyte; bbPC, basement-bridged pericyte; Bp/Vess Length, branch points per vessel length; D, days; FOV, field of view; Frac., fraction; IP Inj., intraperitoneal injection; PCb, pericyte bridge; PCs, pericytes; Post Inj., post-injection; w, weeks.

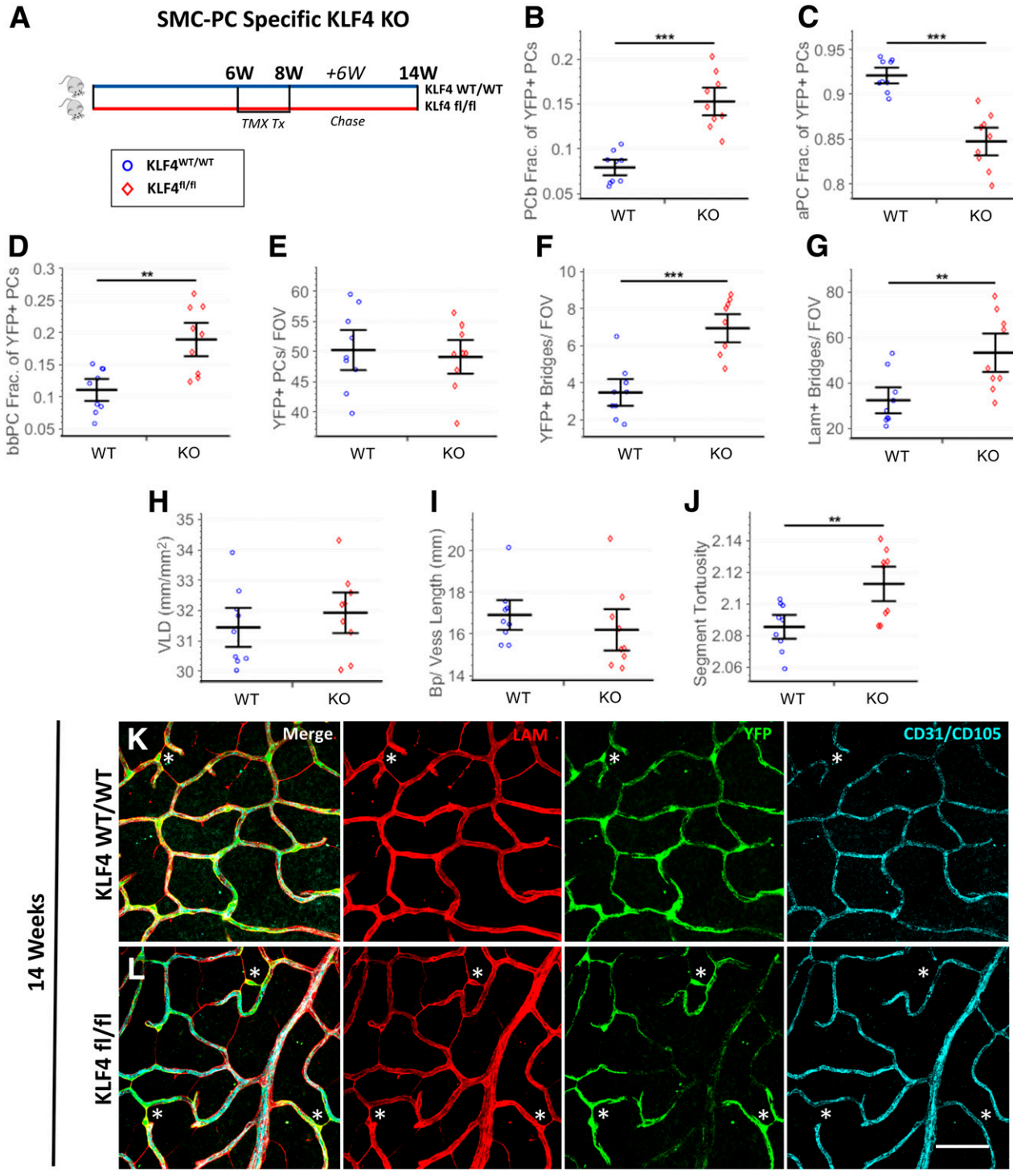

Figure 7—Loss of KLF4 in Myh11 lineage [Myh11-Lin(+)] cells exhibits enriched pericyte bridge density. *A*: Experiment design. In the deep retinal plexus, quantification of Myh11-Lin(+) pericyte morphology, denoted by YFP expression, including fraction of Myh11-Lin(+) pericytes with bridging phenotype (*B*), fraction of Myh11-Lin(+) pericytes with attached phenotype (*C*), fraction of Myh11-Lin(+) pericytes with basement-bridged phenotype (*D*), total Myh11-Lin(+) pericytes per field of view (*E*), Myh11-Lin(+) bridges per field of view (*F*), and all laminin$^+$ bridges per field of view (*G*) (unpaired *t* test; $N = 9$ mice, $n = 4$ images/mouse, 530 μm field of view). Vessel network morphology quantified with vessel length density (VLD) (mm/mm^2) (*H*), number of segments per vessel length (*I*), and vessel segment tortuosity (*J*). *K* and *L*: Representative images of retinal deep plexus from each treatment group 6 weeks after tamoxifen induction stained with anti-laminin (Lam) (red), anti-YFP (green), and anti-CD31 and anti-CD105 (cyan), with annotated pericyte bridges (*) (scale bar, 50 μm). $^{**}P < 0.01$; $^{***}P < 0.001$. aPC, attached pericyte; bbPC, basement-bridged pericyte; Bp/Vess Length, branch points per vessel length; FOV, field of view; Frac., fraction; KO, knockout; PCb, pericyte bridge; PCs, pericytes; Post Inj., post-injection; TMX Tx, tamoxifen treatment; Veh, vehicle; W, weeks.

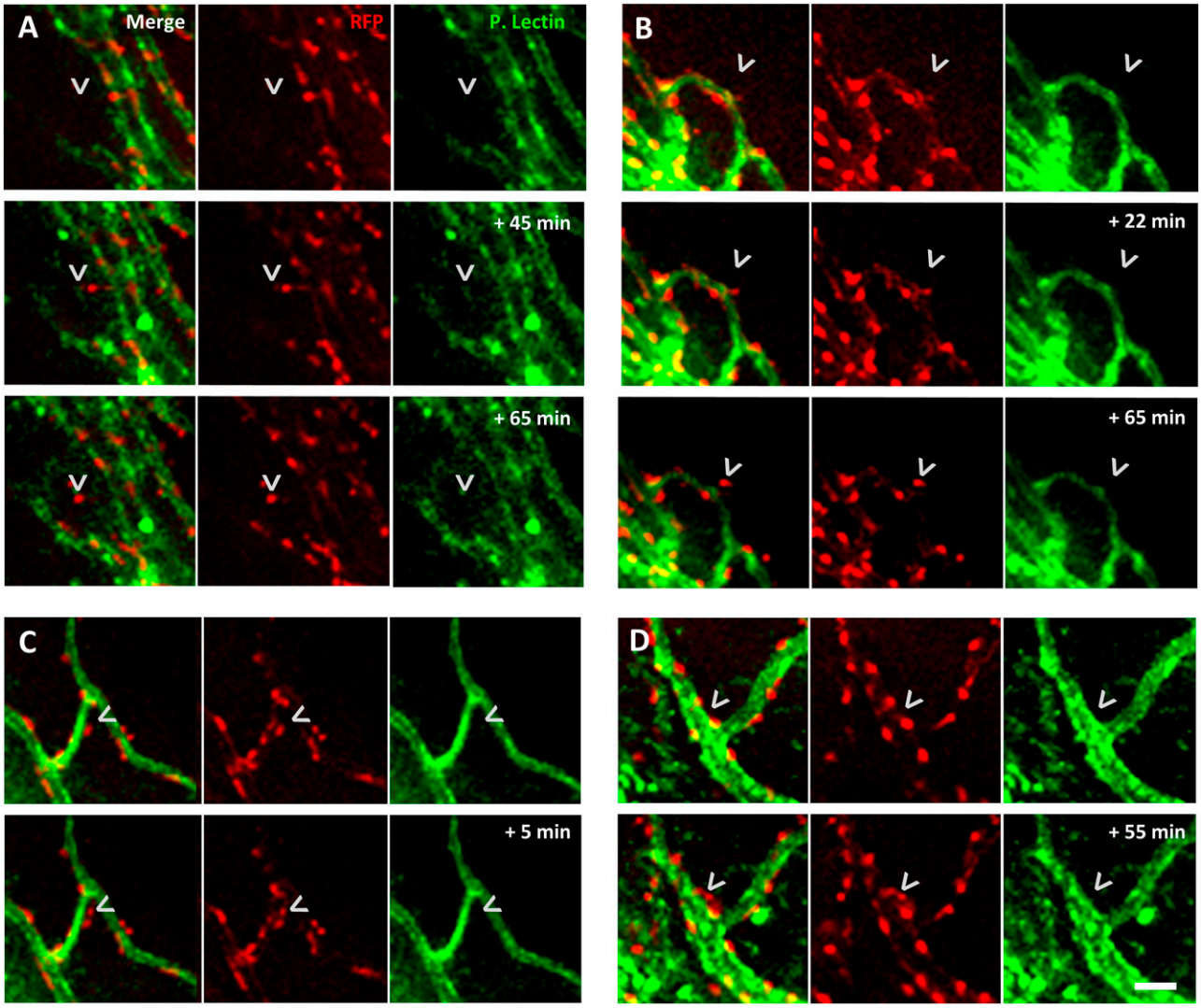

Figure 8— In limbal vessel network, Myh11-lineaged pericytes can detach processes and migrate off vessel visualized through in vivo time lapse. Time-lapse imaging of corneal limbal vessels in Myh11-RFP mouse 2 days post–cornea burn with RFP^+ Myh11-lineaged cells (red) and isolectin IB4–perfused vessels (green). *A–C*: Time lapses that show an RFP^+ cell soma starting fully associated with the vasculature and subsequently migrating off (arrow). *D*: Time lapse of RFP^+ cell extending a process off vessel (arrow) (scale bar, 25 μm).

limited evidence (9–12). Thus, therapeutic interventions have been aimed at mitigating these toxic effects through reduction of high blood glucose, reactive oxygen species, inflammatory cytokines, or angiogenic growth factors (42). The key insight of our study is that there is an early reversible phenotypic shift of pericytes to a bridging cell morphology prior to any net reduction in cell density in response to both hyperglycemia and cytokines upregulated in diabetes. While previous studies have implicated this morphology with diabetic conditions (9–12), the origin of these structures, their underlying function, and their potential contribution to the microvascular pathology associated with diabetes remain unknown.

Our study used definitive lineage markers, time-lapse imaging, genetic models, and extensive microvascular analysis to provide significantly greater insight into the process of bridge formation and its potential role in mediating diabetic vascular damage. We demonstrate that *1*) pericyte-like bridging cells are indeed pericytes, and these cells retain their identity both during and following diabetes and inflammatory stimuli; *2*) individual pericytes can demonstrate bridge formation and off-vessel migration in adult vasculature on a timescale of minutes, and this behavior is reversible; *3*) the microvasculature as a whole exhibits large-scale changes in bridge formation acutely over the course of days, and these changes are reversible; *4*) pericyte bridge formation occurs in diabetic models well in advance of any pericyte or endothelial cell loss; *5*) hyperglycemia-induced elevation in bridge formation and off-vessel pericytes is reversed by administration of insulin; and *6*) pericyte-specific deletion of KLF4,

a transcription factor implicated in restricting cell migration, increases the abundance of pericyte bridges in the retina in the absence of a diabetes microenvironment—demonstrating active, cell-autonomous control of pericyte association with the microvasculature.

Our results strongly support active pericyte detachment as the key mechanism underlying bridge cell and basement membrane bridge formation. Pericyte-like bridge cells are definitively classified as pericytes, given they are marked by a pericyte-specific Myh11 lineage marker and they continue to express Myh11 protein even when their cell body is off vessel. Myh11, a contractile protein, is only found on pericytes and vascular smooth muscle cells (16). Basement membrane bridges spanning between vessels, labeled by Col-IV or laminin, often colabel with antibodies to both Myh11 protein and the pericyte fluorescent lineage marker, indicating active association of a pericyte process with the bridge. Time-lapse imaging of lineage-marked pericytes shows them clearly moving off vessel and frequently extending and retracting filopodia between vessels.

A particularly intriguing finding is that pericyte bridges are increased in response to chronic hyperglycemia months before pericyte loss and vascular regression are usually observed in diabetic models (34), suggesting this could serve as an early vascular marker predictive of future pericyte loss and subsequent vascular damage. This rapid change in pericyte bridge formation is entirely recapitulated by injection of recombinant Ang2 and PDGF-BB—both cytokines upregulated in diabetes (17,18)—and these effects may potentially be synergistic with those mediated by hyperglycemia itself. Elevation of pericyte bridges in Akita mice (10) provides further evidence that high blood glucose could be a stimulus for enrichment of this pericyte phenotype.

There are several potential mechanisms through which these early migratory changes in pericytes may confer increased susceptibility to a toxic diabetes microenvironment. Chronic loss of anchors for the pericyte cell soma to the underlying vascular basement membrane would be expected to increase the likelihood of cell death, as seen with many cell types (43,44). Furthermore, the loss of the close apposition between endothelial cell and pericyte likely disrupts bidirectional trophic paracrine signaling, leaving both cells potentially vulnerable (45). While temporary pericyte dissociation from the vasculature is thought to be requisite for angiogenic sprout formation (46) and basement membrane bridges are hypothesized to offer a preferential route for the rapid growth of new blood vessels (47), chronic activation of this cellular program by hyperglycemia, leaving the pericyte partially off vessel, likely eventually leads to compromised cellular function.

For the first time, we show that the enrichment of pericyte bridges is a reversible process with restoration to basal levels following insulin treatment in STZ-induced hyperglycemia, both on a short-term time scale of days to a long-term timescale of months. The dynamic capacity of pericyte bridges is reinforced by our observations that after exogenous delivery of Ang2 and PDGF-BB, pericyte bridges return to basal levels. That this behavior is pericyte specific is confirmed by induced knockout of KLF4, which precipitates increased bridging cell density. Taken together, these results suggest that pericyte association with the microvasculature is a dynamic rather than passive process.

Given our results showing that Ang2 and PDGF-BB can modulate pericyte attachment, an interesting avenue of research would be determining whether modulation of proangiogenic stimuli of hyperglycemia in the eye may acutely be able to reverse aberrant pericyte migratory behavior thereby restoring diabetic vascular integrity. We speculate that anti-VEGF treatments that have been shown to not only halt, but in some cases partially reverse, diabetic retinopathy (48) may act partially thru this mechanism, since VEGF is known to modulate pericyte apposition to endothelial cells (49,50). Finally, the identification of pericyte dissociation as a potential early event in precipitation of diabetic retinopathy, confirmed by KLF4 knockout, suggests that manipulation of cell adhesion and migration pathways may serve as a new therapeutic approach for preventing or treating this disease.

Our results also reveal shortcomings in the classical retinal digest assay that has been cited as support for pericyte dropout in diabetic conditions (17) and suggest that pericyte loss as a causative factor in diabetic vasculopathies needs to be reexamined, as it has already been in the Akita mouse model (10). Our analysis of immunostained retinas revealed that up to 50% of all pericyte somas were associated with a basement membrane bridge (combination of pericyte bridges and basement-bridged pericytes), which would have been miscounted as endothelial somas (51,52) in the retinal digest assay; this potentially accounts for the ~30% (17) loss in pericyte density observed with this assay in diabetes and Ang2 stimulation. We show that pericytes only occupy a subset of basement membrane bridges, but this cell-specific colocalization is not captured with the histological staining used in retinal digests, limiting the assay's usefulness for quantifying pericyte bridges and total pericyte cell count.

It is important to highlight that the definition of an acellular capillary in retinal digests has not been uniform throughout the years. While many recent publications include the thin basement membrane bridges we have characterized in their definition of a collapsed acellular capillary (14), there is a classical definition that would instead define these structures as fibrous strands based on diameter relative to neighboring capillaries (31). Acellular capillaries are classically defined as basement membrane bridges that lack any cell nuclei and have a diameter at least 20% of surrounding capillaries (29,31). While we observed these thicker lumenized acellular capillaries in adult human retina, we never observed them in our mouse whole

mount immunostaining images across all experiments, which would have been revealed as a Col-IV$^+$ segment of vasculature with the thickness approaching that of a capillary but lacking any endothelial cell markers. Our analysis of human retina suggest an opportunity to separate these basement membrane bridging structures into two distinct classes based on the presence of a basement membrane lumen and the diameter of the basement membrane bridge.

Our study shows that even in early hyperglycemia there are distinct morphologic changes in attachment between pericytes and their underlying endothelial cells. Perhaps as important, these changes occur acutely on a timescale of days following alterations in the retinal environment. Moreover, even in the setting of sustained, chronic hyperglycemia, there is apparently the opportunity to restore pericyte attachment with endothelial cells to potentially provide meaningful improvements in vascular integrity. This finding, if borne out in subsequent study, may be foundational for discovery of additional mechanisms to meaningfully modulate diabetic vascular disease.

Acknowledgments. The authors thank the University of Virginia's vivarium staff for helping to maintain the mouse strains used for this research, along with Anthony Bruce for managing the laboratory of S.M.P. The authors are also grateful for the Advance Microscopy Facility at the University of Virginia for providing the equipment necessary for high-resolution confocal imaging and Hamzah Shariff and Brian Rothemich from the University of Virginia for help with data analysis.

Funding. This study was funded by National Institutes of Health grants R21 EY028868-01, U01AR069393, and U01HL127654; The Hartwell Foundation; and Stanford Allen Discovery Center (to S.M.P.).

Duality of Interest. P.A.Y. has personal financial interest in and employment with RetiVue, LLC, and is a consultant for Genentech/Roche. No other potential conflicts of interest relevant to this article were reported.

Author Contributions. B.A.C. designed and performed experiments and drafted the figures and manuscript with input from all authors. R.W.D. developed software for data analysis. C.M. aided with data analysis, acquisition, and design of experiments. H.C.R. and N.S. aided with design of experiments and acquisition of data. K.F. and R.P. aided with data analysis and acquisition. M.R.K.-G. aided with development of the project and in vivo imaging. W.L.M., J.C., and G.K.O. aided with developing the central thesis of the manuscript. P.A.Y. and S.M.P. supervised the project. All authors discussed the results and contributed to the final manuscript. S.M.P. is the guarantor of this work and, as such, had full access to all the data in the study and takes responsibility for the integrity of the data and the accuracy of the data analysis.

References

1. Ferland-McCollough D, Slater S, Richard J, Reni C, Mangialardi G. Pericytes, an overlooked player in vascular pathobiology. Pharmacol Ther 2017;171:30–42

2. Tilton RG, Hoffmann PL, Kilo C, Williamson JR. Pericyte degeneration and basement membrane thickening in skeletal muscle capillaries of human diabetics. Diabetes 1981;30:326–334

3. Zeng H, Vaka VR, He X, Booz GW, Chen J-X. High-fat diet induces cardiac remodelling and dysfunction: assessment of the role played by SIRT3 loss. J Cell Mol Med 2015;19:1847–1856

4. Simó R, Stitt AW, Gardner TW. Neurodegeneration in diabetic retinopathy: does it really matter? Diabetologia 2018;61:1902–1912

5. Park DY, Lee J, Kim J, et al. Plastic roles of pericytes in the blood-retinal barrier. Nat Commun 2017;8:15296

6. Bergers G, Song S. The role of pericytes in blood-vessel formation and maintenance. Neuro Oncol 2005;7:452–464

7. Lee R, Wong TY, Sabanayagam C. Epidemiology of diabetic retinopathy, diabetic macular edema and related vision loss. Eye Vis (Lond) 2015;2:17

8. Mendes-Jorge L, Llombart C, Ramos D, et al. Intercapillary bridging cells: immunocytochemical characteristics of cells that connect blood vessels in the retina. Exp Eye Res 2012;98:79–87

9. Pfister F, Feng Y, vom Hagen F, et al. Pericyte migration: a novel mechanism of pericyte loss in experimental diabetic retinopathy. Diabetes 2008;57:2495–2502

10. Mäe MA, Li T, Bertuzzi G, et al. Prolonged systemic hyperglycemia does not cause pericyte loss and permeability at the mouse blood-brain barrier. Sci Rep 2018;8:17462

11. Hou Z, Wang X, Cai J, et al. Platelet-derived growth factor subunit B signaling promotes pericyte migration in response to loud sound in the cochlear stria vascularis. J Assoc Res Otolaryngol 2018;19:363–379

12. Lindblom P, Gerhardt H, Liebner S, et al. Endothelial PDGF-B retention is required for proper investment of pericytes in the microvessel wall. Genes Dev 2003;17:1835–1840

13. Kelly-Goss MR, Sweat RS, Azimi MS, Murfee WL. Vascular islands during microvascular regression and regrowth in adult networks. Front Physiol 2013;4:108

14. Brown WR. A review of string vessels or collapsed, empty basement membrane tubes. J Alzheimers Dis 2010;21:725–739

15. Bryson JL, Griffith AV, Hughes B III, et al. Cell-autonomous defects in thymic epithelial cells disrupt endothelial-perivascular cell interactions in the mouse thymus. PLoS One 2013;8:e65196

16. Hess DL, Kelly-Goss MR, Cherepanova OA, et al. Perivascular cell-specific knockout of the stem cell pluripotency gene Oct4 inhibits angiogenesis. Nat Commun 2019;10:967

17. Hammes H-P, Lin J, Wagner P, et al. Angiopoietin-2 causes pericyte dropout in the normal retina: evidence for involvement in diabetic retinopathy. Diabetes 2004;53:1104–1110

18. Langham RG, Kelly DJ, Maguire J, Dowling JP, Gilbert RE, Thomson NM. Over-expression of platelet-derived growth factor in human diabetic nephropathy. Nephrol Dial Transplant 2003;18:1392–1396

19. Salmon M, Gomez D, Greene E, Shankman L, Owens GK. Cooperative binding of KLF4, pELK-1, and HDAC2 to a G/C repressor element in the SM22α promoter mediates transcriptional silencing during SMC phenotypic switching in vivo. Circ Res 2012;111:685–696

20. Shankman LS, Gomez D, Cherepanova OA, et al. KLF4-dependent phenotypic modulation of smooth muscle cells has a key role in atherosclerotic plaque pathogenesis [published correction appears in Nat Med 2016;22:217]. Nat Med 2015;21:628–637

21. Grossman EJ, Lee DD, Tao J, et al. Glycemic control promotes pancreatic beta-cell regeneration in streptozotocin-induced diabetic mice. PLoS One 2010;5:e8749

22. Fiedler U, Scharpfenecker M, Koidl S, et al. The Tie-2 ligand angiopoietin-2 is stored in and rapidly released upon stimulation from endothelial cell Weibel-Palade bodies. Blood 2004;103:4150–4156

23. Lin Z, Sugai JV, Jin Q, Chandler LA, Giannobile WV. Platelet-derived growth factor-B gene delivery sustains gingival fibroblast signal transduction. J Periodontal Res 2008;43:440–449

24. Tual-Chalot S, Allinson KR, Fruttiger M, Arthur HM. Whole mount immunofluorescent staining of the neonatal mouse retina to investigate angiogenesis in vivo. J Vis Exp 2013;77:e50546

25. Powner MB, Vevis K, McKenzie JA, Gandhi P, Jadeja S, Fruttiger M. Visualization of gene expression in whole mouse retina by in situ hybridization. Nat Protoc 2012;7:1086–1096

26. Corliss BA, Ray HC, Patrie JT, et al. CIRCOAST: a statistical hypothesis test for cellular colocalization with network structures [published correction appears in Bioinformatics 2019;35:720–721]. Bioinformatics 2019;35:506–514

27. Schindelin J, Arganda-Carreras I, Frise E, et al. Fiji: an open-source platform for biological-image analysis. Nat Methods 2012;9:676–682
28. Corliss BA, Doty R, Mathews C, Yates PA, Zhang T, Peirce SM. REAVER: improved analysis of high-resolution vascular network images revealed through round-robin rankings of accuracy and precision. 18 July 2019 [preprint]. bioRxiv: 707570
29. Ding L, Cheng R, Hu Y, et al. Peroxisome proliferator-activated receptor α protects capillary pericytes in the retina. Am J Pathol 2014;184:2709–2720
30. Li C, Issa R, Kumar P, et al. CD105 prevents apoptosis in hypoxic endothelial cells. J Cell Sci 2003;116:2677–2685
31. Dagher Z, Park YS, Asnaghi V, Hoehn T, Gerhardinger C, Lorenzi M. Studies of rat and human retinas predict a role for the polyol pathway in human diabetic retinopathy. Diabetes 2004;53:2404–2411
32. Teichert M, Milde L, Holm A, et al. Pericyte-expressed Tie2 controls angiogenesis and vessel maturation. Nat Commun 2017;8:16106
33. Haskins RM, Nguyen AT, Alencar GF, et al. Klf4 has an unexpected protective role in perivascular cells within the microvasculature. Am J Physiol Heart Circ Physiol 2018;315:H402–H414
34. Lai AK, Lo AC. Animal models of diabetic retinopathy: summary and comparison. J Diabetes Res 2013;2013:106594
35. Praidou A, Klangas I, Papakonstantinou E, et al. Vitreous and serum levels of platelet-derived growth factor and their correlation in patients with proliferative diabetic retinopathy. Curr Eye Res 2009;34:152–161
36. Stratman AN, Schwindt AE, Malotte KM, Davis GE. Endothelial-derived PDGF-BB and HB-EGF coordinately regulate pericyte recruitment during vasculogenic tube assembly and stabilization. Blood 2010;116:4720–4730
37. Wang C, Han M, Zhao X-M, Wen J-K. Kruppel-like factor 4 is required for the expression of vascular smooth muscle cell differentiation marker genes induced by all-trans retinoic acid. J Biochem 2008;144:313–321
38. Kelly-Goss MR, Ning B, Bruce AC, et al. Dynamic, heterogeneous endothelial Tie2 expression and capillary blood flow during microvascular remodeling. Sci Rep 2017;7:9049
39. Rogers MS, Birsner AE, D'Amato RJ. The mouse cornea micropocket angiogenesis assay. Nat Protoc 2007;2:2545–2550
40. Cogan DG, Toussaint D, Kuwabara T. Retinal vascular patterns. IV. Diabetic retinopathy. Arch Ophthalmol 1961;66:366–378
41. Hammes H-P, Feng Y, Pfister F, Brownlee M. Diabetic retinopathy: targeting vasoregression. Diabetes 2011;60:9–16
42. Armulik A, Genové G, Betsholtz C. Pericytes: developmental, physiological, and pathological perspectives, problems, and promises. Dev Cell 2011;21:193–215
43. Stupack DG, Cheresh DA. Get a ligand, get a life: integrins, signaling and cell survival. J Cell Sci 2002;115:3729–3738
44. Streuli CH. Integrins and cell-fate determination. J Cell Sci 2009;122:171–177
45. Geevarghese A, Herman IM. Pericyte-endothelial crosstalk: implications and opportunities for advanced cellular therapies. Transl Res 2014;163:296–306
46. Aguilera KY, Brekken RA. Recruitment and retention: factors that affect pericyte migration. Cell Mol Life Sci 2014;71:299–309
47. Mancuso MR, Davis R, Norberg SM, et al. Rapid vascular regrowth in tumors after reversal of VEGF inhibition. J Clin Invest 2006;116:2610–2621
48. Levin AM, Rusu I, Orlin A, et al. Retinal reperfusion in diabetic retinopathy following treatment with anti-VEGF intravitreal injections. Clin Ophthalmol 2017;11:193–200
49. Greenberg JI, Shields DJ, Barillas SG, et al. A role for VEGF as a negative regulator of pericyte function and vessel maturation. Nature 2008;456:809–813
50. Lin S-L, Chang FC, Schrimpf C, et al. Targeting endothelium-pericyte cross talk by inhibiting VEGF receptor signaling attenuates kidney microvascular rarefaction and fibrosis. Am J Pathol 2011;178:911–923
51. Ozaki H, Inoue R, Matsushima T, Sasahara M, Hayashi A, Mori H. Serine racemase deletion attenuates neurodegeneration and microvascular damage in diabetic retinopathy. PLoS One 2018;13:e0190864
52. Pfister F, Wang Y, Schreiter K, et al. Retinal overexpression of angiopoietin-2 mimics diabetic retinopathy and enhances vascular damages in hyperglycemia. Acta Diabetol 2010;47:59–64